ELSEVIER

Thermochimica Acta 280/281 (1996) 289–301

thermochimica acta

The crystallization kinetics of $Fe_{80}Si_4B_{16}$ metallic glass[1]

Emília Illeková

Institute of Physics, Slovak Academy of Sciences, Dúbravská cesta 9, 842 28 Bratislava, Slovakia

Abstract

Differential scanning calorimetry has been used to study the kinetics of crystallization of $Fe_{80}Si_4B_{16}$ metallic ribbon. Continuous heating and isothermal measuring techniques were used. Two overlapping exothermal peaks were always observed. Both processes proceeded by Johnson–Mehl–Avrami crystallization kinetics having temperature- and time-dependent activation energies. In the first crystallization step $E_1^*(755\,K) = 325$ kJ (g atom)$^{-1}$ continuously increased to $E_1^*(794\,K) = 487$ kJ (g atom)$^{-1}$ and the exponent $n_1 = 2.5$ decreased to 1.5 for extended degrees of conversion. These observations were interpreted as crystallization of two types of primary product having quite different kinetics. In the second crystallization step the exponent $n_2 = 4$ and the activation energy E_2^* having the mean value of 340 kJ (g atom)$^{-1}$ decreased slightly with increasing temperature. These observations were interpreted as the crystallization of the metastable and stable eutectic phases.

Keywords: Crystallization kinetics; DSC; $Fe_{80}Si_4B_{16}$; Johnson–Mehl–Avrami kinetics; Metallic glass

1. Introduction

The excellent soft magnetic properties of metallic glasses have found use in many industrial applications and new glasses and their technological potential are continually being explored. It has recently been shown that in certain FeSiB glasses small volume fractions of suitable additives uniformly distributed within the amorphous matrix further improve the magnetic properties of the nanostructured products of their partial crystallization, named FINEMET [1–3]. Successful exploitation of this effect requires detailed understanding of the crystallization process in these precursors because, in particular, the influence of annealing temperature on the types of phases that crystal-

[1] Dedicated to Professor Hiroshi Suga.

0040-6031/96/$15.00 © 1996 – Elsevier Science B.V. All rights reserved
SSDI 0040-6031(95)02649-5

lize, their spatial distribution and the kinetics of the nucleation and growth processes have been observed in FeSiB glasses [4–6].

The recent structural models of FeSiB glasses are based on the short-range, ordered clusters surrounded by the amorphous matrix having a structure not yet described. The relationship between the ordering inside the clusters in the amorphous matrix and the future crystals is not yet known. The crystallization of such a complicated non-equilibrium solid structure at temperatures much lower than that of equilibrium crystallization is seen to be a complicated multiprocess in time and temperature. Both isothermally and in a continuous heating regime several processes cooperate.

The crystallization behaviour of several FeSiB glasses has been studied using a variety of techniques. The authors in Ref. [7] characterized the thermal stability, effective activation energies E_1^* and Avrami exponents n_1 of the first crystallization step, and, in Ref. [8], the second stage of the crystallization also, of a large variety of FeSiB glasses using differential scanning calorimetry (DSC). In Ref. [9] high-temperature magnetization and X-ray diffraction studies were performed. Several different types of primary product of the first crystallization step and two types of eutectic, stable and metastable, crystallizing during the second crystallization step in FeSiB metallic glasses were observed and examined in detail by transmission electron microscopy (TEM) [4–6]. The influences of alloy composition and annealing temperature and time on the crystallization behaviour and the crystallization products were indicated.

Power-compensated DSC has proved to be a very sensitive tool for the investigation of the kinetics of thermally activated processes such as crystallization in non-crystalline solids. Despite this, large variability is obtained in measurements of crystallization parameters characterizing the same crystallization step of some glasses, namely metallic alloys. Their dependence on the kinetic analysis method used (differential or integral), the thermal history of the sample, and therefore also on the measuring regime (isothermal or non-isothermal) is evident for FeSiB glasses also [6].

In this paper the DSC study of the complex two-step crystallization of $Fe_{80}Si_4B_{16}$ metallic glass is presented. The crystallization experiments were performed by combining both continuous heating and isothermal measuring regimes. The Johnson–Mehl–Avrami (JMA) kinetic equation was applied to each step separately. The apparent activation energies E_i^* and the JMA exponents n_i $(i = 1, 2)$ were calculated by the Kissinger method and by the fitting of both continuous heating and isothermal DSC peaks. The temperature, T, time, t, and degree of conversion, α, dependences of $E_i^*(T, t, \alpha)$ and $n_i(T, t, \alpha)$ were tested by the isoconversional method.

The work described here is a part of a continuing investigation of the thermodynamic stability of FeSiB-based metallic ribbons [10].

2. Experimental

The 23 μm thick $Fe_{80}Si_4B_{16}$ metallic ribbons were prepared by the planar flow casting technique (the quenching rate $\beta^- \sim -10^7\ K\ s^{-1}$). Their non-crystalline nature was tested by X-ray diffraction and electron microscopy. The measurements of as-quenched samples were performed with a Perkin–Elmer DSC 7 instrument using

a continuous heating regime with heating rates, β^+, from 10 to 80 K min^{-1}, and an isothermal regime with a heating ramp with $\beta^+ = 40$ K min^{-1}. In both cases the quasi-linear temperature-dependences of the specific heats of the samples, $C_p(T)$, excluding the transformation peaks in the first measuring run, and in the whole second measuring run (in relation to the height of the transformation peaks) were indicated. Pronounced initial transient effects in both first and second isothermal measuring runs were observed. Therefore the first measuring run only was always used for the kinetic calculations. Samples (5 mg) were cut into small pieces, and covered with the Al lid; an empty Al pan reference and a dynamic argon atmosphere were used.

The temperature and enthalpy axes of the DSC instrument were calibrated by the use of indium and zinc standards for all heating rates. Afterwards no heating rate influence on the Curie point of nickel was observed.

3. Results and discussion

3.1. Dynamic heat treatment

A series of DSC experiments was carried out on the $Fe_{80}Si_4B_{16}$ ribbons with continuous heating rates in the range 10–80 K min^{-1}. The crystallization of the glassy sample was always characterized by two overlapping exothermal peaks. In addition, the shape of the overall thermogram was dependent on the heating rate. As shown in Fig. 1, the ratio of the heights and also of the partial enthalpies of the two peaks increased continuously with heating rate from 0.68 or 0.67, respectively, (at $\beta^+ = 10$ K min^{-1}) to 4.49 or 5.79, respectively (at $\beta^+ = 80$ K min^{-1}). This phenomenon has already been observed [6].

3.2. Isothermal heat treatment

A series of isothermal DSC experiments was carried out on the ribbons at temperatures T_a in the range 753–783 K which is related to the onset temperature of the first dynamic crystallization DSC peak ($T_x = 777$ K at $\beta^+ = 10$ K min^{-1}). Two well separated exothermal peaks were always observed (Fig. 2).

3.3. Kinetic analysis

The difference between the glass-like and crystal-like specific heats of $Fe_{80}Si_4B_{16}$ is very small relative to the heights of the crystallization apparent specific heat peaks. (The glass transition region is not visible.) The straight lines between the first and last points could be thus used as the baseline for ΔH_{cryst} and $\alpha(T,t) = \Delta H(T,t)/\Delta H_{cryst}$ calculations. ΔH_{cryst} and $\Delta H(T,t)$ are the total and partial transformation enthalpies, which are the temperature or time integrals of the measured DSC signal dH/dT or dH/dt. $\alpha(T,t)$ is the kinetic degree of conversion. The first and second crystallization steps (which will be named R1 and R2 in the following) are assumed to be independent and the kinetic equations were applied to each step separately. This assumption is valid

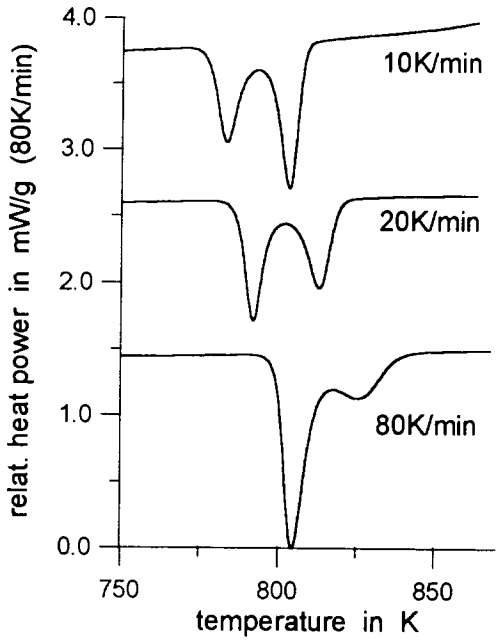

Fig. 1. The continuous heating DSC traces of crystallization of $Fe_{80}Si_4B_{16}$ ribbon at various heating rates (being the parameter). The y scales were modified in proportion to the rates.

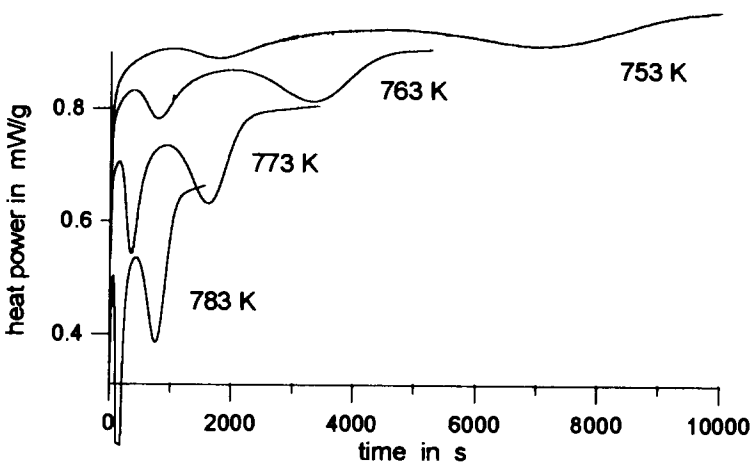

Fig. 2. The isothermal DSC traces of crystallization of $Fe_{80}Si_4B_{16}$ ribbon at various annealing temperatures (being the parameter).

in the isothermal situation as can be seen from Fig. 2. But a certain deformation of $\alpha(T)$ resulting from any dynamic DSC peak signal is evident, as can be seen from Fig. 1, the R1 and R2 processes always overlap in temperature and the last R1 signal point being the first R2 signal point (without any deconvolution of the measured signal into two

ideal peaks) does not reach the height of the common smooth $C_p(T)$ baseline modulating both peaks.

For the study of crystallization kinetics we assume, as is usual in the case of metallic glasses, that each crystallization peak can be described by a kinetic equation of the form

$$d\alpha/dt = k(T)f(\alpha) \tag{1}$$

where

$$k(T) = A\exp[-E^*/(RT)], \tag{2}$$

is the Arrhenius temperature-dependent rate constant, E^* is the apparent activation energy, and A is the pre-exponential factor. $f(\alpha)$ characterizes the T- or β^+-independent- type of transformation mechanism.

On the basis of the dynamic DSC measurements at various heating rates the Kissinger peak method [11] was used to deduce the apparent activation energies E^*_{Ki} for R1 and R2. The slopes of $\ln(\beta^+/T^2_{pi})$ vs $1/T_{pi}$ dependences being E^*_{Ki}, where T_{pi} are the R1 and R2 peak maxima temperatures, are in both cases systematically increasing with β^+ (Fig. 3). The mean value of E^*_{K1} is 487 kJ (g atom)$^{-1}$ and E^*_{K2} is 458 kJ (g atom)$^{-1}$ and their physical sense will be discussed later.

Accurate complex kinetic treatment of all peaks was hindered by their overlapping. However, the isothermal and also certain dynamic DSC measurements enabled us to deduce the values of $f(\alpha)$, E^* and A for R1 and R2 without any additional assumption. The general kinetic equation, Eq. (1) can be rewritten in the logarithmic form as

$$\ln(d\alpha/dt) - \ln A + E^*/RT = \ln[f(\alpha)] \tag{3}$$

The right side of Eq. (3) depends neither on T nor on β^+. The left side of the equation is, except for some constant, directly the DSC signal ($d\alpha/dt = 1/\Delta H_{cryst} dH/dt$). Then the vertical shift d of the $\ln(d\alpha/dt)$ representation of two of the isothermal measurements at

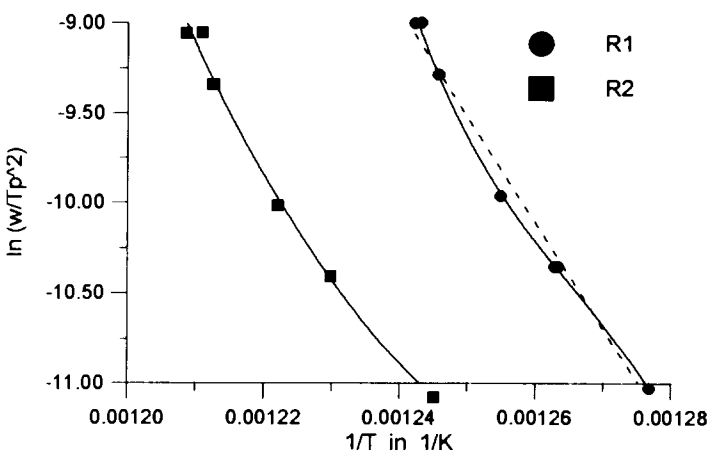

Fig. 3. Kissinger plots of the first and second crystallization steps for $Fe_{80}Si_4B_{16}$ ribbon.

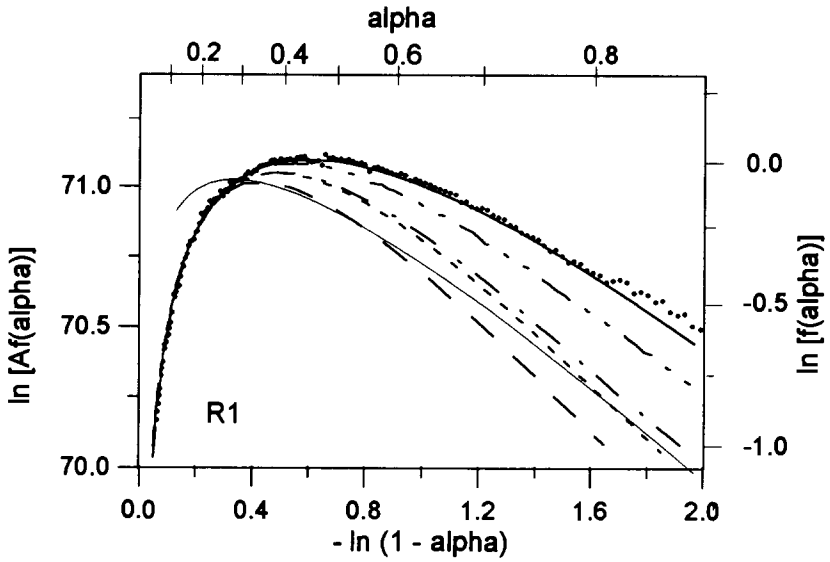

Fig. 4. Plots of $\ln[A\mathrm{f}(\alpha)], = \ln(\mathrm{d}\alpha/\mathrm{d}t) + E^*/RT$ or $\ln(\mathrm{d}\alpha/\mathrm{d}T) + E^*/RT + \ln\beta^+$ in the isothermal or continuous heating mode, eventually, versus $-\ln(1-\alpha)$ for the first crystallization step in $Fe_{80}Si_4B_{16}$ ribbon under different experimental conditions. Isotherms at temperatures: ....., 753; -..-..-, 758; -.-.-, 773 K. Dynamic measurements at heating rates: ---, 10; ——, 60 K min^{-1}. Dark and light continuous lines are theoretical curves obtained for JMA kinetic equations with exponents $n = 2.5$ and 1.5, respectively.

different temperatures is proportional to E^*:

$$d = \ln(\mathrm{d}\alpha/\mathrm{d}t)_{T_\mathrm{I}} - \ln(\mathrm{d}\alpha/\mathrm{d}t)_{T_\mathrm{II}} = (E^*/R)(1/T_\mathrm{II} - 1/T_\mathrm{I}) \quad (4)$$

In the case of R1 the systematic increase of E_1^* from 325 kJ (g atom)$^{-1}$ to 433 kJ (g atom)$^{-1}$ with increasing T_a from 753 to 783 K was calculated and its physical sense will be discussed later (see Fig. 8). In the case of R2 the mean value of slightly decreasing E_2^* with increasing T_a is $E_2^* = 340$ kJ (g atom)$^{-1}$.

As expected, the kinetic equations become different from each other when their $\mathrm{f}(\alpha)$ dependences are represented in an appropriate coordination system as, for example, a plot of $\ln[\mathrm{f}(\alpha)]$ versus $-\ln(1-\alpha)$, as it was shown by Suriñach et al. in Fig. 5 of Ref. [12]. (Alternatively, Šatava's integral method [13] for non-isothermal curve fitting, where $\ln[\int_0^\alpha(\mathrm{d}\alpha'/\mathrm{f}(\alpha'))]$ depends on $1/T$ or the classical Avrami method [14] for isothermal JMA curve fitting, where $\ln(-\ln(1-\alpha))$ depends on $\ln(t_a - \tau)$ and where τ is an appropriate linearization time constant, could have been used [15].) The dependences of $\ln[A\mathrm{f}(\alpha)]$ being equivalent to $\ln(\mathrm{d}\alpha/\mathrm{d}t) + E^*/RT$ or $\ln(\mathrm{d}\alpha/\mathrm{d}T) + E^*/RT + \ln\beta^+$ on $-\ln(1-\alpha)$, obtained from the isotherms of Fig. 2 or dynamic DSC curves from Fig. 1, respectively, for R1 are shown in Fig. 4. Those for R2 are shown in Fig. 5. The dotted lines represent the experimental results and the full lines the values calculated by the use of Johnson–Mehl–Avrami (JMA) kinetic model for $\mathrm{f}(\alpha)$, namely $\mathrm{f}(\alpha) = n(1-\alpha)[-\ln(1-\alpha)]^{(n-1)/n}$. There is good agreement between the experimental points and the

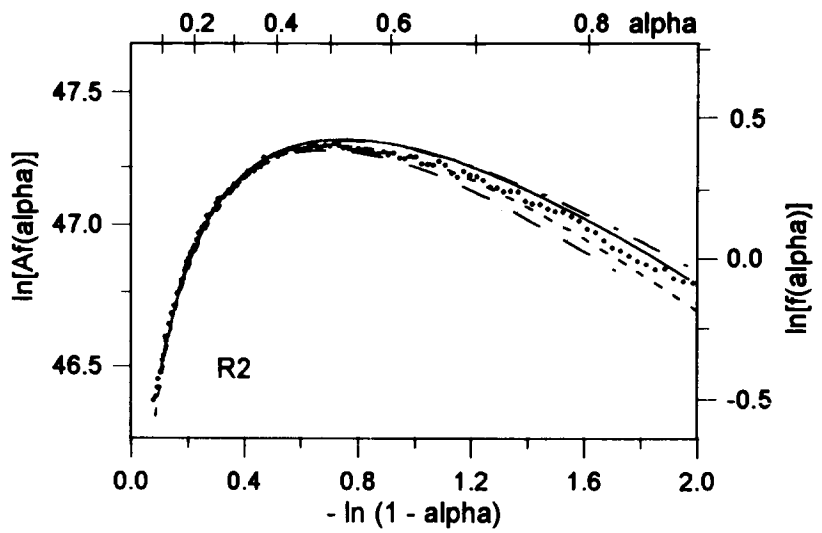

Fig. 5. Plots of $\ln[A\mathrm{f}(\alpha)], = \ln(\mathrm{d}\alpha/\mathrm{d}t) + E^*/RT$ or $\ln(\mathrm{d}\alpha/\mathrm{d}T) + E^*/RT + \ln\beta^+$ in the isothermal or continuous heating mode, eventually, versus $-\ln(1-\alpha)$ for the second crystallization step in $Fe_{80}Si_4B_{16}$ ribbon under different experimental conditions. Isotherms at temperatures: ...., 753; -.-.-, 773 K. Dynamic measurements at heating rates: – – –, 10; ——, 20 K min^{-1}. Solid line, theoretical curve obtained for JMA kinetic equation with exponent $n = 4$.

values predicted by this model with $n_1 = 2.5$ (homogeneous nucleation and diffusion-controlled three-dimensional growth) for the initial parts of the R1 crystallization step independently of annealing temperature T_a or heating rate β^+. At higher T_a and $\alpha_1 > 0.5$ or higher β^+ and $\alpha_1 > 0.35$ the exponent continuously decreases to reach $n_1 = 1.5$. This systematic shift of n_1 at elevated α_1 during dynamic experiments significantly exceeds the error caused by the incorrect baselines. In the case of R2 there is excellent agreement between the values predicted by the JMA model with $n_2 = 4$ (homogeneous nucleation and interface reaction controlled three-dimensional growth) for all isothermal events and dynamic experiments with low β^+. At $\beta^+ > 20$ K min^{-1} both the difference between the through (unknown) and assumed baselines and the overlapping of R1 exceeded the height of the DSC peak signal and hindered the determination of any meaningful kinetic information (making E^*_{K2} doubtful also).

Once E^* and $\mathrm{f}(\alpha)$ are known, the vertical difference b between any of the either isothermal or dynamic DSC signals modified by the third term of the left side of Eq. (3) and the model $\mathrm{f}(\alpha)$ dependence gives $\ln A$. The systematically increasing A_1 from 6.9×10^{19} to 8.0×10^{26} s^{-1} with increasing T_a, the mean value of $\bar{A}_1 = 7.1 \times 10^{30}$ s^{-1} for dynamic experiments and the mean values of $\bar{A}_2 = 2.7 \times 10^{20}$ s^{-1} were calculated. These results together with those deduced for E^*_1 and E^*_2 reflect the mutual dependence of the Arrhenius parameters known as the kinetic compensation effect [16].

Similarly, JMA kinetics with transient nucleation [14] and three-dimensional growth for both R1 and R2 crystallization steps and the mean value of exponent

$\tilde{n}_2 = 3.45$, $E^*_{\tau 2} = 352$ kJ (g atom)$^{-1}$ for the early stages of R2 and $E^*_{JMA,2} = 311$ kJ (g atom)$^{-1}$ and $A_2 = 1.1 \times 10^{18}$ s^{-1} for the advanced stages of the R2 process in $Fe_{80}Si_4B_{16}$ ribbon were derived when the isothermal DSC signals were represented in $\ln(-\ln(1-\alpha))$ vs $\ln(t_a - \tau)$ coordinates [17].

In the case of well defined kinetics the T and α dependences in the kinetic equation can be separated. To verify this the constancy of the deduced model parameters (E^*, n or A) has to be tested. From Eq. (1) at any moment (T_α, t_α) of the proceeding transformation having a constant degree of conversion α, independently of T_a or β^+, it follows that

$$\ln(d\alpha/dt)_\alpha = \text{const} - E^*/(RT_\alpha). \tag{5}$$

Then, using the so-called isothermal isoconversional method (the expanded Friedman method [18]), the slope of the measured DSC signals at various T_a, $\ln(dH/dt)_\alpha$ vs $1/T_a$ gives the activation energy $E^*_I(\alpha)$, or, using the continuous heating isoconversional method in the case of several continuous heating curves at various β^+, the slope of $\ln(dH/dT)_\alpha$ vs $1/T_\alpha$ gives $E^*_{CH}(\alpha)$. In such a complex isothermal study of our R1 crystallization step the effective activation energy was found to be satisfactorily independent of α reaching the mean value of $\bar{E}^*_{I1}(\alpha_1 \leq 0.6) = 503$ kJ (g atom)$^{-1}$ for $\alpha_1 \leq 0.6$, which slightly exceeds the values of E^*_I deduced from previous curve fitting. Later (for $\alpha_1 > 0.6$) probably some other process (R2) is contributing, drastically minimizing E^*_I and simultaneously increasing the dispersion of the data (see Fig. 6). In the case of R2 the effective activation energy was $\bar{E}^*_{I2}(\alpha_2 \leq 0.8) = 252$ kJ (g atom)$^{-1}$

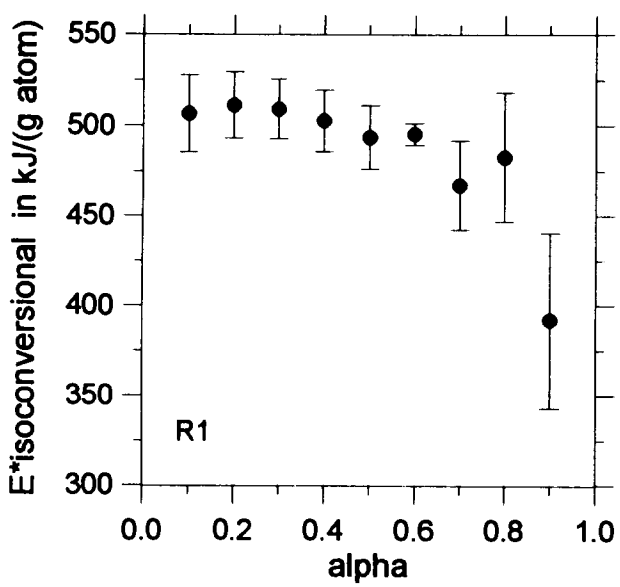

Fig. 6. The dependence of the isoconversional-method-calculated activation energy of the first isothermal crystallization peak of $Fe_{80}Si_4B_{16}$ ribbon on the degree of conversion α_1.

relatively independent of α_2 for practically the whole transformation (see Fig. 7). However its absolute value is very low. In the continuous heating regime the situation was much more complicated, probably because of the presence of several processes in both R1 and R2 crystallization steps, their mutual overlapping and incorrect integration baselines. The apparent activation energies (which in the case of isoconversional method are in every moment resulting from the whole integration of all dynamic DSC curves measured at different β^+) strongly depended on α and did not reach any realistic absolute value.

4. Interpretation

Our DSC experiments showed a systematic variation with heating rate in the shape of the thermogram for $Fe_{80}Si_4B_{16}$, in that the first peak, R1—associated with primary crystallization—became relatively more prominent than the second peak R2—associated with the eutectic crystallization—with increasing temperature. The JMA exponents n_i which are well defined in the initial stages of both processes, continuously decrease with temperature and/or time. Similar effects with time were found to operate during isothermal annealing at different temperatures. Also, strong temperature-dependences of effective E_i^* were always observed.

All values of the parameters n_i, A_i and E_i^* calculated from the fitting of our dynamic and isothermal thermograms of R1 and R2 crystallization steps in $Fe_{80}Si_4B_{16}$ ribbon

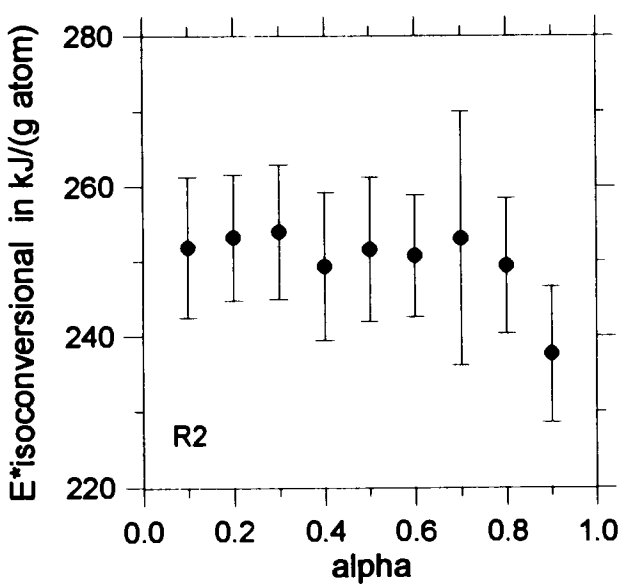

Fig. 7. The dependence of the isoconversional-method-calculated activation energy of the second isothermal crystallization peak of $Fe_{80}Si_4B_{16}$ ribbon on the degree of conversion α_2.

are summarized in Table 1. The eventual temperature-dependence of E_1^* can be deduced from Fig. 8. Similar absolute values and mutual relations have been published for other FeSiB ribbons in [5, 7, 8, 10, 19].

Our observed dependences in the case of R1 correlate with the microstructural analysis of Gibson and Delamore [6] which showed that at all heating rates and

Table 1
Kinetic data of the $Fe_{80}Si_4B_{16}$ metallic ribbon

Peak	n_i	A_i/s^{-1}	E_i^*(755 K)/(kJ (g atom)$^{-1}$)	E_i^*(760 K)/(kJ (g atom)$^{-1}$)	E_i^*(778 K)/(kJ (g atom)$^{-1}$)	E_{Ki}^*/(kJ (g atom)$^{-1}$)	E_i^*/(kJ (g atom)$^{-1}$)
R1	2.5[a]	–[b]	325	345	433	487 ± 20	503 ± 9[c]
R2	4	2.7×10^{20}	346	341	334	458 ± 24[d]	252 ± 1

[a] For $\alpha_1 > \alpha_{1,\text{critical}}$ (which critical extent of conversion is temperature-dependent) $n_1 = 1.5$.
[b] Increasing from 6.9×10^{19} at $T_a = 753$ K to 8.0×10^{26} at $T_a = 783$ K for isothermal regimes and 7.1×10^{30} for dynamic measuring regimes.
[c] For $\alpha_1 \leq 0.6$.
[d] Of low reliability.

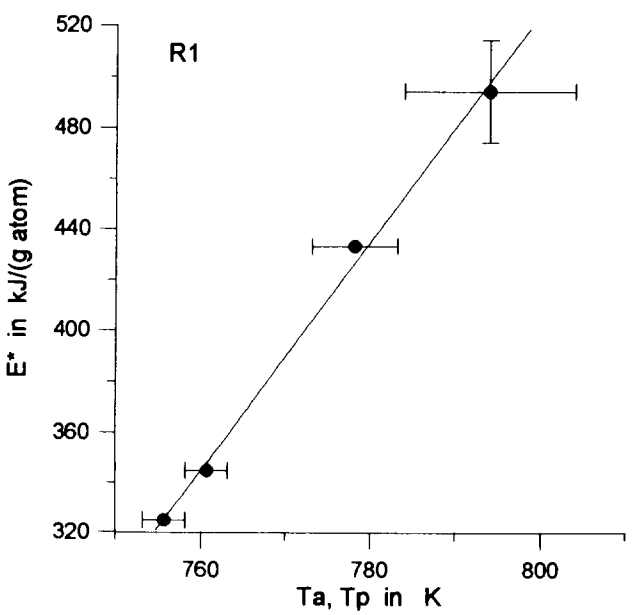

Fig. 8. The temperature-dependence of the activation energy calculated for the first crystallization step in $Fe_{80}Si_4B_{16}$ ribbon. T_a, the annealing temperatures of isothermal experiments; T_p, the peak temperatures from the dynamic experiments.

annealing temperatures the primary crystallization product of R1 is a mixture of simple α-Fe(Si) dendrites and more complicated particles consisting of an Fe_3B core surrounded by α-Fe(Si) isolating it from the amorphous matrix. The content of these composite crystals increases with increasing temperature and thus reduces the amorphous content of the rest of the matrix. The transformation kinetics of these two types of R1 product are quite different. The simple α-Fe(Si) shows, after some incubation time, a linear increase in crystal numbers with time at each annealing temperature (transient homogeneous nucleation). The composite crystals are related to some quenched-in sites within the matrix. After an appropriate incubation time, during the annealing these clusters tend to establish their equilibrium distribution reaching the size of the Fe_3B nuclei. Thereafter the Fe_3B crystals start to grow; these in turn, after some time, heterogeneously nucleate the stable α-iron phase. After a certain exhaustion time, when the quenched-in sites in the matrix are exhausted, this nucleation mechanism stops (transient heterogeneous nucleation). Comparing these results with our curves in Fig. 4 it is clear that the observed absolute value and α_1-dependence of the total $n_1(\alpha_1)$ closely resembles the JMA crystallization process with homogeneous nucleation superimposed on JMA crystallization with heterogeneous nucleation. (In Figs. 4 and 5 the incubation times were already subtracted before any curve fitting, therefore we cannot see the transient effects there). Annealing the sample at $T_a = 753$ K the α-Fe(Si) crystallization ($n_1 = 2.5$) dominates. On the other side in the case of dynamic crystallization having $\beta^+ = 80\,\mathrm{K\ min^{-1}}$ the growth of the already saturated heterogeneous nucleation (saturating at $\alpha_1 \sim 0.3$) of the composite crystals ($n_1 = 1.5$) dominates.

In the case of R2 regular JMA crystallization with homogeneous nucleation and interface-controlled three-dimensional growth of the remaining amorphous matrix ($n_2 = 4$) was always realized. The apparent temperature-dependence of its effective activation energy E_2^* has to be interpreted. TEM photomicrography of fully transformed ribbon sample isothermally annealed has shown [4] that the microstructure of $Fe_{80}Si_4B_{16}$ consists of a large volume fraction of non-faceted α-Fe(Si) dendrites in an α-Fe + Fe_2B eutectic matrix. The morphology of the eutectics is fine and irregular. We have mentioned that during R1 a certain amount of Fe_3B was already crystallized (being the core of the composite crystals) diminishing the content of the remaining amorphous matrix. In fact recent work [5] has shown that certain glassy alloys in the system Fe–Si–B can crystallize in the second crystallization step to either stable α-Fe + Fe_2B or metastable α-Fe + Fe_3B eutectics. So in our case also some competition between these stable and metastable eutectics evidently depends on temperature, in favour of the stable one with increasing temperature. Fe_3B resulting from the probable metastable eutectic reaction and/or a certain amount of Fe_3B already crystallized in the first crystallization stage have to decompose into the finally observed Fe_2B and α-Fe(Si), depending on temperature, parallel to the R2 crystallization step. In fact no additional peaks in the DSC traces, neither in temperature nor in time were observed. A similar conclusion comes from the magnetization and X-ray observations of Singhal and Majumdar [9] where a certain temperature interval was measured between the appearance of the Fe_3B and Fe_2B ferromagnetic contributions during the dynamic crystallization of $Fe_{80}Si_4B_{16}$ ribbon.

5. Conclusions

In this paper both dynamic and isothermal DSC investigation of the crystallization of $Fe_{80}Si_4B_{16}$ ribbon is presented. Two exothermal peaks, R1 and R2, were always observed. The mutual relationship between their shapes, overlapping and kinetics was temperature-dependent.

The $\ln(d\alpha/dt) + E^*/RT$ or $\ln(d\alpha/dT) + E^*/RT + \ln\beta^+$ vs $-\ln(1-\alpha)$ representation of the measured thermograms was found to be a sensitive method for determining the kinetics of both R1 and R2 processes. Regular JMA kinetics were always deduced (not assuming further empirical models [20]).

The R1 step is primary crystallization of α-Fe(Si) phase with transient homogeneous nucleation and primary crystallization of composite crystals of Fe_3B and α-Fe(Si) with transient heterogeneous nucleation. The three-dimensional growth of both types of particle is diffusion-controlled. At low temperatures (in the case of isothermal annealing) the first type of precipitation dominates while at high temperatures (in the dynamic experiments) the second type of precipitation dominates and the exhaustion time of its nucleation shortens. Therefore an increase of the effective JMA activation energy E_1^* with increasing temperature and a decrease of JMA effective exponent n_1 with time are observed.

The final products of the total transformation of $Fe_{80}Si_4B_{16}$ ribbon are the stable α-Fe (Si) and Fe_2B crystals.

The R2 step proceeds by homogeneous nucleation and three-dimensional linear growth of the stable and metastable eutectics. The competition between these stable α-Fe + Fe_2B and metastable α-Fe + Fe_3B eutectics and simultaneous transformation of the already existing Fe_3B to Fe_2B results in the slight decrease of the effective activation energy E_2^* both with increasing temperature and time.

Because of temperature-dependent effective activation energies $E_i^*(T)$ of both R1 and R2 processes, the apparent activation energies $E_{Ii}^*(\alpha)$ calculated by the isoconversional method representing the integral information from a wide temperature interval possess only qualitative information (in relation to $E_i^*(T)$). This must also be taken into account in the case of Kissinger activation energies E_{Ki}^*.

Acknowledgements

The author is grateful to Dr. P. Duhaj for the preparation of the metallic ribbons, to the Dipartimento di Fisica, Universita di Ferrara, (Italy) for financial support and to F. Malizia for assistance with the measurements.

References

[1] Y. Yoshizawa, S. Oguma and K. Yamauchi, J. Appl. Phys., 64 (1988) 6044.
[2] Y. Yoshizawa, K. Yamauchi, T. Yamana and H. Sugihara, J. Appl. Phys., 64 (1988) 6047.
[3] G. Gerzer, Phys. Scr., 49 (1993) 307.

[4] M.A. Gibson and G.W. Delamore, Mat. Sci. Eng., A117 (1989) 255.
[5] M.A. Gibson and G.W. Delamore, Acta Metall., 38 (1990) 2621.
[6] M.A. Gibson and G.W. Delamore, J. Mater. Sci., 27 (1992) 2533.
[7] V.R.V. Ramanan and G.E. Fish, J. Appl. Phys., 53 (1982) 2273.
[8] S. Suriñach, M.D. Baró and N. Clavaguera, Z. Phys. Chem. Neue Folge, 157 (1988) 395.
[9] R. Singhal and A.K. Majumdar, J. Magnet. Magnet. Mater., 115 (1992) 245.
[10] E. Illeková, F. Malizia and F. Ronconi, Thermochim. Acta, submitted for publication.
[11] H.E. Kissinger, Anal. Chem., 29 (1957) 1702.
[12] S. Suriñach, M.D. Baró, M.T. Clavaguera-Mora and N. Clavaguera, J. Non-Cryst. Solids, 58 (1983) 209.
[13] J. Šesták, V. Šatava and W.W. Wendlandt, Thermochim. Acta, 7 (1973) 333.
[14] C.V. Thompson, A.L. Greer and F. Spaepen, Acta Metall., 31 (1983) 1883.
[15] None of the known kinetics gives a linear $\ln[\int_0^x (d\alpha'/f(\alpha'))]$ versus $1/T$ or $\ln(-\ln(1-\alpha))$ versus $\ln(t_a - \tau)$ curve fit in the case of crystallization of metallic glasses ([E. Illeková, P. Ambrovič and P. Duhaj, Amorphous Metall. Mater., 5 (1980) 165]; [10]). Because of the shape of the $\ln[f(\alpha)]$ versus $-\ln(1-\alpha)$ curve fitting and the position of its maximum, in the case of JMA kinetics using Suriñach's method [12], it is more sensitive to choose the most probable one than the linearization curve fitting in Šatava's or Avrami's procedures.
[16] N. Koga and J. Šesták, Thermochim. Acta, 182 (1991) 201.
[17] E. Illeková, unpublished results.
[18] T. Ozawa, J. Therm. Anal., 31 (1986) 547.
[19] N. Kunitomi, Mater. Sci. Eng., A179/180 (1994) 293.
[20] J. Šesták and J. Málek, Solid State Ionics, 63/65 (1993) 245.